ADVANCED ENERGY MATERIALS
www.advenergymat.de

www.MaterialsViews.com

A Novel High-Energy Hybrid Supercapacitor with an Anatase TiO_2–Reduced Graphene Oxide Anode and an Activated Carbon Cathode

*Haegyeom Kim, Min-Young Cho, Mok-Hwa Kim, Kyu-Young Park, Hyeokjo Gwon, Yunsung Lee, Kwang Chul Roh, and Kisuk Kang**

A hybrid supercapacitor with high energy and power densities is reported. It comprises a composite anode of anatase TiO_2 and reduced graphene oxide and an activated carbon cathode in a non-aqueous electrolyte. While intercalation compounds can provide high energy typically at the expense of power, the anatase TiO_2 nanoparticles are able to sustain both high energy and power in the hybrid supercapacitor. At a voltage range from 1.0 to 3.0 V, 42 W h kg^{-1} of energy is achieved at 800 W kg^{-1}. Even at a 4-s charge/discharge rate, an energy density as high as 8.9 W h kg^{-1} can be retained. The high energy and power of this hybrid supercapacitor bridges the gap between conventional batteries with high energy and low power and supercapacitors with high power and low energy.

1. Introduction

Energy-storage devices delivering high energy and power have a wide range of applications, from renewable energy storage to hybrid electric vehicles (HEVs).[1–9] Increasing demands from these sectors are now requiring better-performing energy-storage concepts.[10–20] Among conventional energy-storage devices, lithium ion batteries (LIBs) can provide high energy density (~150 W h kg^{-1}) as a result of Faradaic reactions derived from the intercalation of large numbers of lithium ions into the electrodes. However, intrinsically slow solid-state lithium diffusion in the bulk and the accompanying volumetric strain has limited its high-power capability.[21–23] On the other hand, supercapacitors can provide good power (2–5 kW kg^{-1}) as a result of fast surface reactions, while they suffer from low energy density (3–6 W h kg^{-1}) because charge is stored only on the surface.[21,24–26] For emerging new applications, the current status of energy storage using LIBs or supercapacitors barely satisfies the demands in terms of both energy and power; thus, bridging the performance gap between LIBs and supercapacitors is becoming an important issue in the field of energy storage.

To combine the advantages of LIBs and supercapacitors, a new concept—i.e., a hybrid supercapacitor—was recently proposed.[21,24] The hybrid supercapacitor uses a Faradaic lithium-intercalation cathode (such as $LiMn_2O_4$) or anode (such as $Li_4Ti_5O_{12}$), which are commonly used as LIB electrodes, and combines it with a non-Faradaic capacitive anode or cathode (typically a carbonaceous material), which are used in supercapacitors, in a non-aqueous electrolyte (**Figure 1**).[27,28] The hybrid supercapacitor asymmetrically and simultaneously stores charges by surface ion adsorption/desorption on one electrode and by lithium de/intercalation in the other electrode. The combination of the Faradaic intercalation and non-Faradaic surface reaction provides an opportunity to effectively improve the energy and power densities.[21]

One of the major issues for hybrid supercapacitors, however, is the imbalance in the power capability between the two electrodes. Faradaic lithium-intercalation is far more sluggish than a non-Faradaic capacitive reaction. At normal operating conditions of a hybrid supercapacitor, this imbalance in the kinetics prevents full energy utilization of the intercalation electrode and imposes a high overpotential in the capacitive electrode, thus deteriorating the overall efficiency. Therefore, balancing of the kinetics—in particular, by enhancing the power capability of the Faradaic lithium-intercalation electrode—is of utmost importance to the performance of the hybrid supercapacitor.

In order to remedy the sluggish reaction of the intercalation electrode in the hybrid supercapacitor, in this study we employed anatase TiO_2 nanoparticles embedded in reduced graphene oxide as the anode. While the electrochemical performance of anatase TiO_2 in the hybrid supercapacitor with non-aqueous electrolyte has not previously been reported, nanosized anatase TiO_2 is regarded as a promising anode for LIBs[29,30] because of

H. Kim, K.-Y. Park, H. Gwon, Prof. K. Kang
Department of Materials Science and Engineering
Research Institute of Advanced Materials (RIAM)
Seoul National University
599 Gwanak-ro, Gwanak-gu, Seoul, Republic of Korea
E-mail: matlgen1@snu.ac.kr
M.-Y. Cho, M.-H. Kim, Dr. K. C. Roh
KICET, 233-5 Gasan-dong, Guemcheon-Gu, Seoul 153-801
Republic of Korea
Prof. Y. Lee
Faculty of Applied Chemical Engineering
Chonnam National University
Gwangju 500-757, Republic of Korea
Prof. K. Kang
Center for Nanoparticle Research
Institute for Basic Science (IBS)
Seoul National University
Seoul 151-742, Republic of Korea

DOI: 10.1002/aenm.201300467

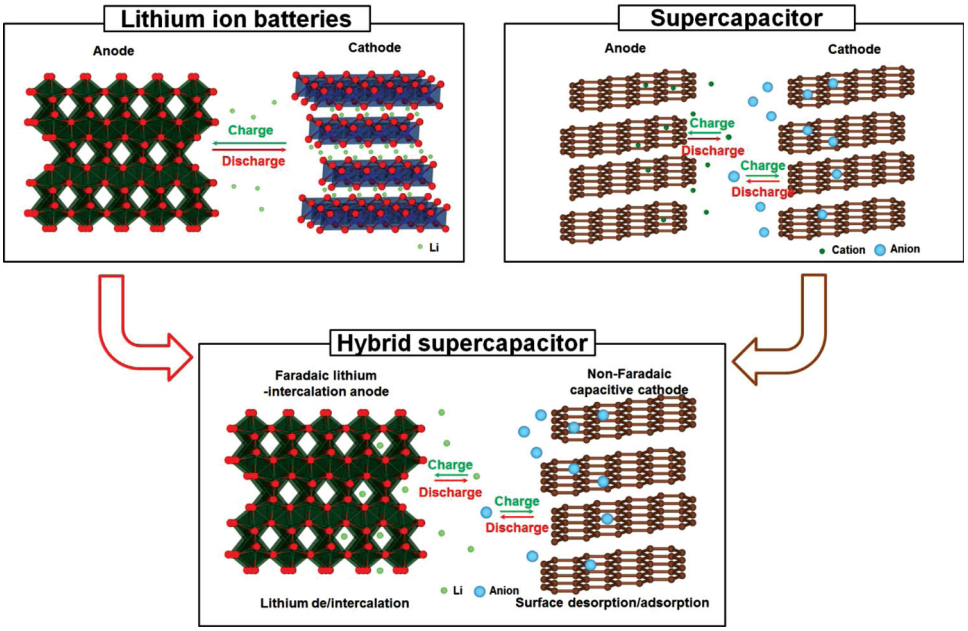

Figure 1. Illustration of a typical hybrid supercapacitor. The hybrid supercapacitor uses a non-Faradaic capacitive cathode like those used in supercapacitors and a Faradaic lithium-intercalation anode like those used in LIBs.

its low potential, good cycle stability, and fast lithium intercalation.[31–33] Here, we demonstrate that the use of TiO_2 anchored on reduced graphene oxide can substantially increase the performance of hybrid supercapacitors, delivering 42 W h kg^{-1} at 800 W kg^{-1} and 8.9 W h kg^{-1} even at a 4-s charge/discharge rate. This new system based on anatase TiO_2 and reduced graphene oxide may be the key to bridge the gap between high-energy LIBs and a high-power supercapacitors.

2. Results and Discussion

TiO_2-containing reduced graphene oxide was synthesized in a simple process during the reduction of graphene oxide (GO), as described in the Experimental Section. All X-ray diffraction (XRD) peaks (**Figure 2**a) could be indexed with those of anatase TiO_2 without any impurities (Joint Committee on Powder Diffraction Standards, JCPDS card no. 21-1272). A calculation

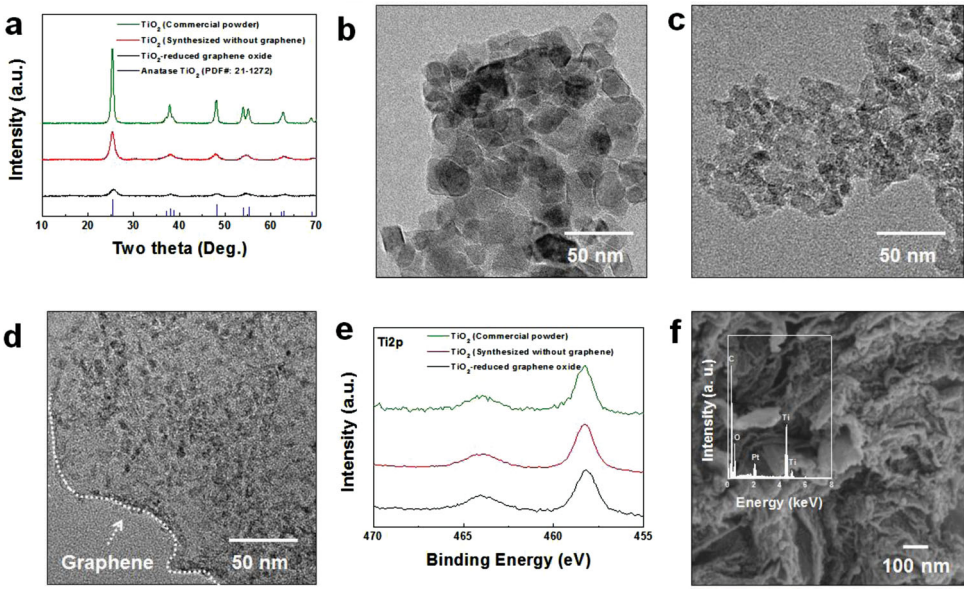

Figure 2. Characterization of TiO_2–(reduced graphene oxide). a) XRD plots of TiO_2–(reduced graphene oxide), TiO_2 nanoparticles synthesized without reduced graphene oxide, and commercial TiO_2 powder. b–d) HR-TEM images of commercial TiO_2 powder (b), TiO_2 nanoparticles synthesized without reduced graphene oxide (c), and TiO_2–(reduced graphene oxide) (d). e) XPS spectra in the Ti 2p region. f) FE-SEM image of TiO_2–(reduced graphene oxide). Inset: EDS analysis. The presence of Pt detected by EDS originated from the Pt coating of the sample for SEM analysis.

Table 1. Full-width at half-maximum of the (101) plane and the equivalent particle size calculated from Scherrer's equation.

	Full-width at half-maximum [°]	Equivalent particle size [nm]
TiO_2–(reduced graphene oxide)	1.306	6.2
TiO_2 (Synthesized without graphene)	0.84	9.68

using Scherrer's equation gave an equivalent particle size of 6.2 nm for the TiO_2 within the reduced graphene oxide, which is smaller than the TiO_2 nanoparticles synthesized in a similar manner but without reduced graphene oxide (9.68 nm), as presented in **Table 1**.[34–36] The high-resolution transmission electron microscopy (HR-TEM) analysis of the morphology and particle size of TiO_2–(reduced graphene oxide) confirmed that the particle size of the TiO_2 on the reduced graphene oxide was ~5 nm, which is more than twice as small as that of TiO_2 without reduced graphene oxide (~10 nm) or that of battery-grade commercial TiO_2 (~20 nm) (Figure 2b–d). This indicated that the use of reduced graphene oxide promoted the formation of smaller TiO_2 nanoparticles. We attribute this behavior to the defects on the reduced graphene oxide surface that may provide heterogeneous nucleation sites for facile TiO_2 formation.[34,37,38] Because the heterogeneous nucleation is faster than homogeneous nucleation, the growth of particles is comparatively suppressed. Thus, extremely small TiO_2 particles formed on the reduced graphene oxide. Using high-magnification field-emission scanning electron microscopy (FE-SEM) and HR-TEM (Figure S1 in the Supporting Information, SI), it was found that TiO_2 nanoparticles are grown on the reduced graphene oxide, specifically at the edges and wrinkled regions of the graphene layers. Because edges and wrinkled regions contain lots of defects and have higher surface energy, TiO_2 nanoparticles prefer to grow at those sites to heal defects and reduce surface energy. X-ray photoelectron spectroscopy (XPS) peaks in the Ti 2p region agreed well with those of pure anatase TiO_2, indicating the defect-free anatase phase on the reduced graphene oxide (Figure 2e).[39] Figure 2f is an FE-SEM image of the TiO_2–(reduced graphene oxide) sample in which the wrinkled nature of the reduced graphene oxide is evident. The rough surface of the reduced graphene oxide likely originated from the presence of the TiO_2 nanoparticles. Energy dispersive spectroscopic (EDS) analysis further confirmed that anatase TiO_2 was present on the wrinkled reduced graphene oxide (inset in Figure 2f). The reduction of the particle size led to higher surface area. Brunauer–Emmett–Teller (BET) analysis indicated that the surface area of the TiO_2–(reduced graphene oxide) sample was 405.9229 $m^2\ g^{-1}$, whereas the surface areas of TiO_2 nanoparticles without reduced graphene oxide and that of the commercial powder are 221.3402 and 58.0225 $m^2\ g^{-1}$, respectively. The chemical structure of reduced graphene oxide was further analyzed by XPS (Figure S2, SI). It was confirmed that only small amounts of functional groups such as C–O and C=O remains in the reduced graphene oxide, indicating that functional groups were effectively removed by chemical reduction using NH_2NH_2 followed by heating at 400 °C. Before constructing a full-cell, the lithium-storage capability of TiO_2–(reduced graphene oxide) was examined in a Li half-cell over 1.0 to 3.0 V (**Figure 3**a,b). The

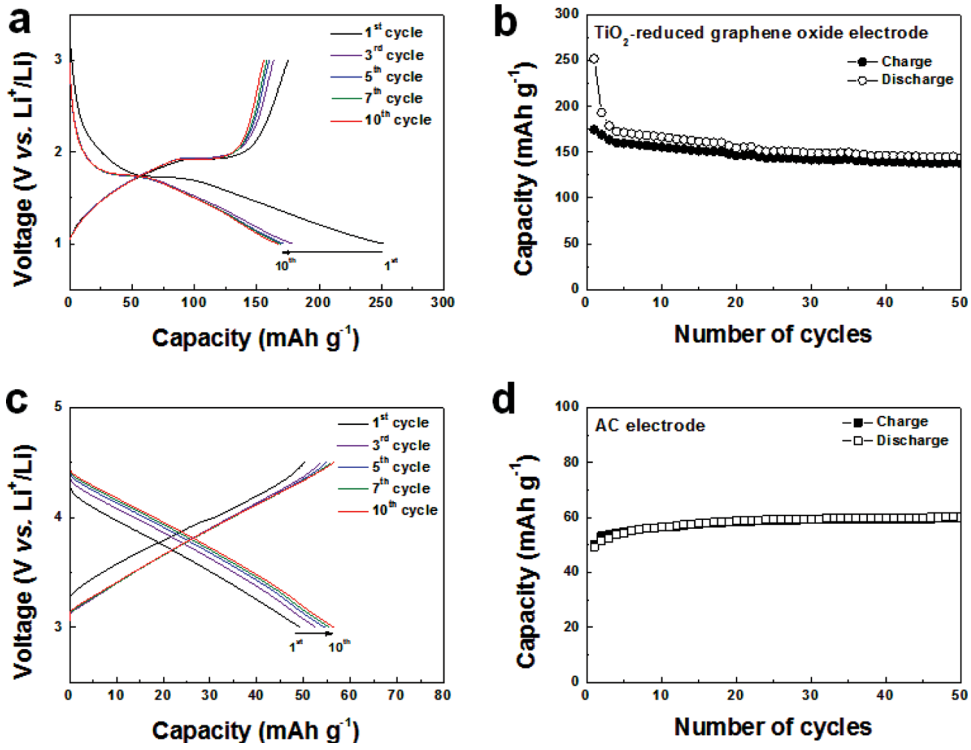

Figure 3. Electrochemical performance of TiO_2–(reduced graphene oxide) and AC electrodes in a Li half-cell. a) Charge/discharge profiles for the initial 10 cycles and b) the cyclability of the TiO_2–(reduced graphene oxide) electrode in the voltage window of 1.0–3.0 V at a current rate of 0.2 A g^{-1}. c) Charge/discharge profiles for the initial 10 cycles and d) cyclability of the AC electrode in the voltage window of 3.0–4.5 V at a current rate of 0.2 A g^{-1}.

characteristic plateau around 1.7 V in Figure 3a indicates reversible intercalation of Li into the anatase TiO_2 structure. At a current rate of 200 mA g^{-1} (>1*C*, where current rate 1*C* = 168 mA g^{-1}), TiO_2–(reduced graphene oxide) retained a high specific capacity of about 145 mA h g^{-1} (~88% of the theoretical capacity) after 50 cycles. During repeated battery cycling, the charge/discharge profiles did not change significantly, indicating that the de/intercalation reaction was highly reversible. The charge/discharge properties of the activated carbon (AC) electrode in a Li half-cell system were also measured at a current rate of 200 mA g^{-1} over 3.0 to 4.5 V as shown in Figure 3c; Figure 3d shows its cycle stability. The linear charge/discharge profiles revealed that the AC electrode operated by a characteristic non-Faradaic capacitive reaction, in which the charge/discharge process occurred with the adsorption/desorption of ions on the surface.[40] The AC electrode had an acceptably high capacity of ~55 mA h g^{-1} with the reversible surface reaction on the AC electrode.

The electrochemical performance of the TiO_2–(reduced graphene oxide) electrode in the hybrid supercapacitors was then investigated. The hybrid supercapacitors were constructed using an anode of TiO_2–(reduced graphene oxide) and a cathode of AC. The cyclic voltammetry (CV) analysis was carried out for the TiO_2–(reduced graphene oxide)//AC hybrid supercapacitor system from 1.0 to 3.0 V at scan rates from 2.0 to 20.0 mV s^{-1}. While an ideal symmetric supercapacitor shows rectangular CV profiles,[41] **Figure 4**a(i) shows that the CV profile of the TiO_2–(reduced graphene oxide)//AC hybrid supercapacitor had two different regions. To better understand this behavior, CV analyses of Li half-cells using the TiO_2–(reduced graphene oxide) electrode (ii) and the AC electrode (iii) were performed at a scan rate of 2.0 mV s^{-1}. The TiO_2–(reduced graphene oxide) electrode showed distinct peaks, which were attributed to the redox reaction of TiO_2, while the AC electrode exhibited a rectangular CV shape. This indicated that both capacitive and redox reactions occurred in the hybrid supercapacitors. In the hybrid supercapacitor system, the redox peaks in the CV resulted from the oxidation and reduction of Ti^{4+} ions in the TiO_2–(reduced graphene oxide) electrode.[42–44] Notably, the decrease in overpotential when the hybrid supercapacitor was constructed compared to the TiO_2–(reduced graphene oxide) electrode is attributed to the kinetic difference between the reversible surface–anion adsorption/desorption reaction and the ionization/precipitation reaction of Li metal. The specific capacitances of TiO_2 nanoparticles without reduced graphene oxide and commercial powder were also measured and compared with that of TiO_2–(reduced graphene oxide) using the following relationship:[40]

$$C = \frac{q}{\Delta V \times m} = \frac{\int i \Delta t}{\Delta V \times m} \quad (1)$$

where *C* is the capacitance (F g^{-1}), ΔV is the voltage change, *m* is the mass of the active materials in both electrodes, *q* is the total charge obtained by the integration of positive and negative sweeps of the CV analysis (Figure S3, SI), *i* is the current, and *t* is time. The capacitances of the hybrid supercapacitor containing the TiO_2–(reduced graphene oxide) electrode were 89, 75, 63, and 53 F g^{-1} at scan rates of 2.0, 5.0, 10.0, and 20.0 mV s^{-1}, respectively. These capacitances were substantially higher than those of TiO_2 nanoparticles, as shown in Figure 4b. The higher capacitances were attributed to the higher surface area provided by the smaller anatase TiO_2 particles.

The electrochemical performance was also measured by galvanostatic charge/discharge at current densities from 0.4 to 4.0 A g^{-1}. Figure 4c shows the charge/discharge profiles of the samples at a current rate of 0.4 A g^{-1}. They did not follow the typical triangular profiles, unlike symmetric AC/AC supercapacitors, because they underwent the charge transfer reaction of the battery-type lithium-intercalation. This behavior confirmed again that the charge storage in the hybrid supercapacitor combined the capacitor and battery mechanisms.[41] The discharge specific capacitances of the hybrid supercapacitor using the TiO_2–(reduced graphene oxide) anode were about 150, 90, 70, 55, 50, and 30 F g^{-1} at current rates of 0.4, 0.8, 1.2, 1.6, 2.0, and 4.0 A g^{-1}, respectively (Figure S4, SI). These values were more than three times higher than those of TiO_2 nanoparticles without reduced graphene oxide or those of battery-grade commercial TiO_2 powder. The high specific capacitance was well maintained up to 10 000 cycles, except for the initial 100 cycles (Figure 4d). The initial specific capacitance of ~150 F g^{-1} decreased to ~120 F g^{-1} (80% of the initial value) after 100 cycles at a current density of 0.4 A g^{-1}. However, outstanding retention of the specific capacitance was achieved after the first 100 cycles.

In order to further evaluate the practical applicability of the hybrid supercapacitor system, a Ragone plot was constructed from the galvanostatic capacitance data (**Figure 5**). The specific power density (*P*) and energy density (*E*) of the hybrid supercapacitor were calculated as follows:[40,45]

$$P = \Delta V \times I/m \quad (2)$$

$$E = P \times t/3600 \quad (3)$$

$$\Delta V = (E_{max} + E_{min})/2 \quad (4)$$

where E_{max} and E_{min} are the potentials at the beginning and the end of the discharge (V), respectively, *I* is the charge/discharge current (A), *t* is the discharge time (s), and *m* is the mass of active materials including both the anode and cathode in the hybrid supercapacitor. The Ragone plot demonstrated that the hybrid supercapacitor containing TiO_2–(reduced graphene oxide) delivered one of the highest specific power and energy densities among similar systems.[21,27,40,45–47] The maximum specific energy density of this system was 42 W h kg^{-1} at a specific power of 800 W kg^{-1}. It also delivered about 8.9 W h kg^{-1} at a specific power density of 8000 W kg^{-1}, which is three to four times higher than the control groups. Even when comparing with previously reported high-performance hybrid systems using lithium-intercalating electrode materials with non-aqueous electrolytes, the superior performance of the hybrid supercapacitor with the TiO_2–(reduced graphene oxide) anode is quite notable. For comparison, the energy and power densities of TiO_2–(B)nanowires//carbon nanotubes (CNT),[21] $LiTi_2(PO_4)_3$//AC,[45,46] V_2O_5//CNT,[40] $Li_4Ti_5O_{12}$//AC,[27] and $LiCrTiO_4$//AC[47] are plotted together in Figure 5; the graph clearly shows that the hybrid supercapacitor based on (anatase TiO_2)–(reduced graphene oxide) can deliver far higher power and energy densities. For a more realistic consideration, gravimetric energy and power is typically

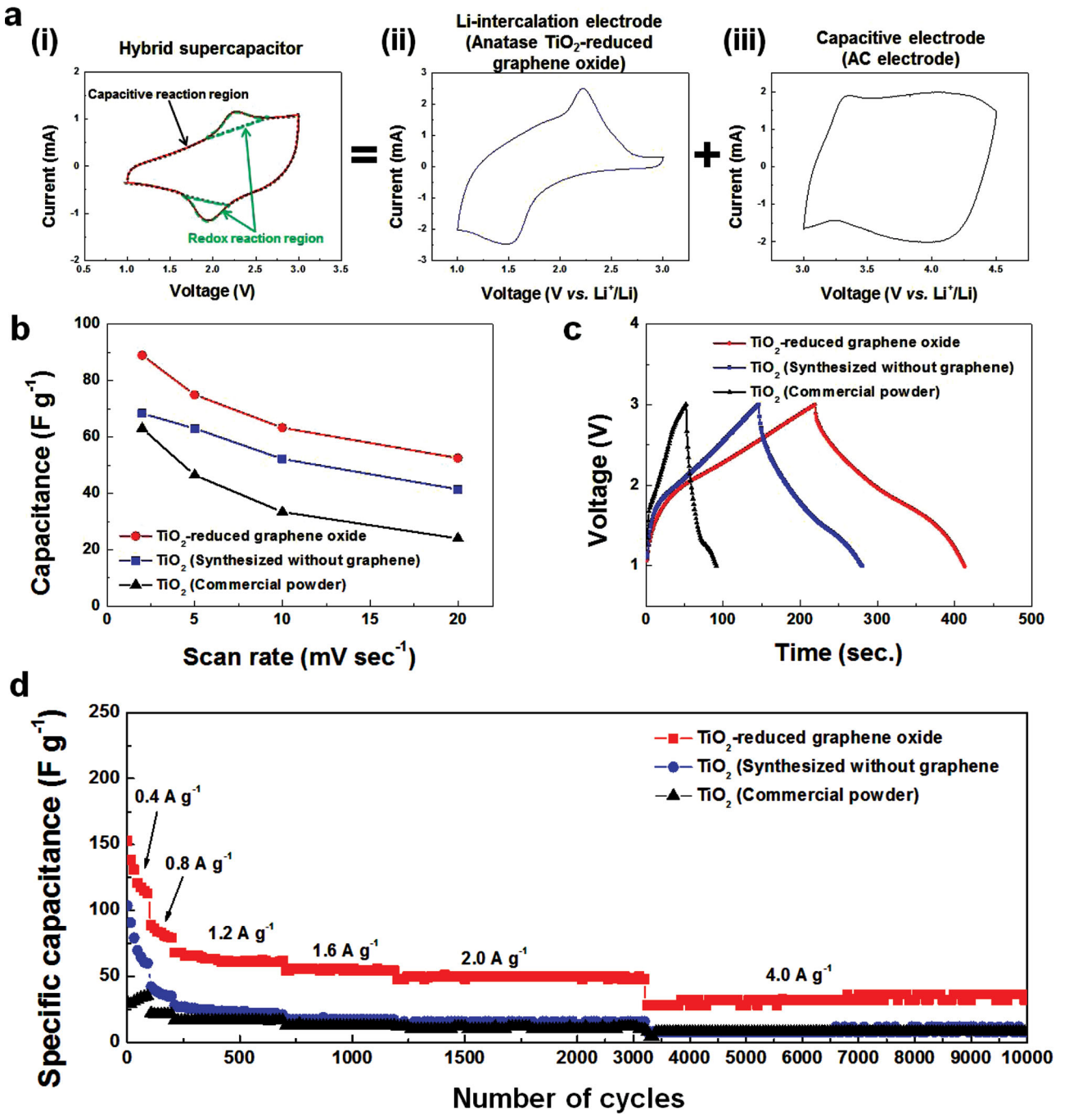

Figure 4. Electrochemical performance of TiO_2–(reduced graphene oxide) in the hybrid supercapacitor. a) CV analysis of i) the hybrid supercapacitor based on the TiO_2–(reduced graphene oxide) anode and AC cathode and of ii,iii) TiO_2–(reduced graphene oxide) (ii) and AC electrodes (iii) in a Li half-cell. b) Specific capacitance of TiO_2–(reduced graphene oxide) and TiO_2 nanoparticles in the hybrid supercapacitor. c) Initial charge/discharge profiles of the hybrid supercapacitor. d) Cyclability and rate capability of the hybrid supercapacitor at various current rates, from 0.4 to 4.0 A g^{-1}.

estimated for a practical cell construction by dividing the values of the energy and power densities of the electrode by a factor of ~2.[48,49] The Ragone plot for such a realistic cell is shown in Figure S5 (SI); it reveals that both the energy and power levels of our system approached the requirements for an HEV application.[50]

The high energy and power characteristics of the TiO_2–(reduced graphene oxide)//AC hybrid supercapacitor were attributed to the following aspects. i) The reasonably low flat potential at ~1.7 V increased the cell voltage compared to AC/AC symmetric supercapacitors, enhancing the energy density of the system (Figure S6, SI). ii) The unique TiO_2–(reduced

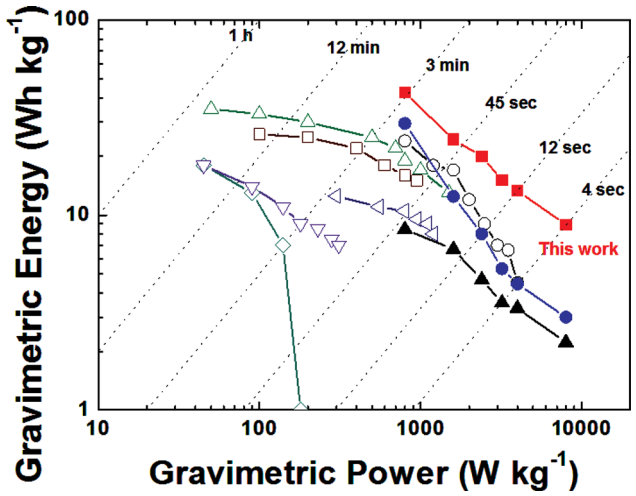

Figure 5. Ragone plots of various hybrid supercapacitors. The hybrid supercapacitor based on the TiO_2–(reduced graphene oxide) anode delivered dramatically improved energy and power densities. Hybrid supercapacitors based on TiO_2–(reduced graphene oxide)//AC (■), TiO_2 nanoparticles without reduced graphene oxide (●), and commercial TiO_2 powder (▲) are compared with other hybrid supercapacitor systems using TiO_2–(B)nanowires//carbon nanotubes (CNT) (◁);[21] $LiTi_2(PO_4)_3$//AC (◇),[45] (□);[46] V_2O_5//CNT (▽);[40] $Li_4Ti_5O_{12}$//AC (△);[27] and $LiCrTiO_4$//AC (○).[47]

graphene oxide)nanostructure substantially improved the electrochemical kinetics. Reduced graphene oxide promoted the facile synthesis of extremely small anatase TiO_2 particles with their high electrical conductivity and high surface area. Also, a conductive network was provided throughout the electrode, thereby enhancing the electrochemical reaction.[34,37,38] The conductive framework effectively decreased the internal resistance of TiO_2 electrode, as evidenced from the electrochemical impedance spectroscopic measurements (Figure S7, SI). In this way, the comparatively inferior rate capability of TiO_2 to the non-Faradaic AC cathode at high current rates could be significantly overcome. In general, we believe that the suitable design of the electrode architecture providing networked electron pathways is one of the promising approaches to improve electrochemical performance of electrode materials.[51,52] Finally, iii) nanosized TiO_2 particles shortened the ion diffusion length and so reduced the ionic diffusion resistance and charge transfer resistance.[53]

3. Conclusion

A new hybrid supercapacitor comprising an anatase TiO_2–(reduced graphene oxide) anode and an AC cathode exhibited a promising energy-storage capability that could bridge the gap between conventional LIBs and supercapacitors. The energy density of the new system (42 W h kg^{-1}) was one of the highest among hybrid supercapacitor systems based on intercalation compounds. The energy and power densities could satisfy the requirements of an HEV application. With optimization, this new system could be a strong competitor for energy storage in HEVs.

4. Experimental Section

Fabrication of Graphene Oxide: Graphite oxide was synthesized using a modified Hummers method.[54] Graphite (1 g), $NaNO_3$ (1 g), and H_2SO_4 (46 mL) were stirred together in an ice bath for 30 min, followed by slow addition of $KMnO_4$ (5 g). The mixture was stirred for 2 h at 50 °C. Deionized (DI) water (100 mL) and H_2O_2 (30%, 8 mL) were then added to the mixture. Filtering and washing with HCl (30%, 50 mL) and DI water (200 mL) allowed isolation of the graphite oxide. To obtain graphene oxide (GO), the graphite oxide was dissolved in DI water (1 mg/mL, 400 mL) and sonicated for 100 min. During this process, graphene oxide layers were exfoliated from the graphite oxide.

Fabrication of TiO_2–(Reduced Graphene Oxide): Titanium tetrachloride ($TiCl_4$) was used as a precursor to synthesize the TiO_2–graphene. $TiCl_4$ (2 M, 4 mL) was slowly added to a graphene oxide solution (1 mg/mL, 400 mL). NH_4OH (4 mL) and NH_2NH_2 (35 wt%, 0.4 mL) were then added to reduce the graphene oxide. The solution was stirred for 6 h at 80 °C and filtered. The resultant powder was heated to 400 °C to obtain the final product, TiO_2–(reduced graphene oxide).

Characterization of TiO_2–(Reduced Graphene Oxide): TiO_2–(reduced graphene oxide) was analyzed by XRD (D2 PHASER) with Cu Kα radiation and by XPS (PHI 5000 VersaProbe). The morphology of the samples was studied by FE-SEM (SUPRA 55VP) and by HR-TEM (JEM–3000F). The surface area of the prepared TiO_2–(reduced graphene oxide) was quantified by the BET method. The graphene content of the TiO_2–(reduced graphene oxide) was analyzed by an element analyzer (EA, Fisions EA-1110), which established 5.32 wt% of carbon in the composite.

Electrochemical Testing of TiO_2–(Reduced Graphene Oxide): Electrodes were prepared by mixing the TiO_2–(reduced graphene oxide) (80 wt%) with conductive carbon (10 wt%) and polyvinylidene fluoride (PVDF) (10 wt%) in *N*-methyl-2-pyrrolidone (NMP) for electrochemical characterization. The resultant slurries were uniformly applied to Al foil. The electrodes were dried at 120 °C for 2 h and roll-pressed. An AC electrode was prepared by mixing AC (MSP-20, 90 wt%) with conductive carbon (5 wt%) and polytetrafluoroethylene (PTFE, 5 wt%). For half-cell tests, cells were assembled into two-electrode cells with a Li metal counter electrode, a separator (Celgard 2400), and an electrolyte of lithium hexafluorophosphate (1 M) in a 1:1 mixture of ethylene carbonate and dimethyl carbonate (Techno Semichem) in a glove box. For full-cell tests of the hybrid supercapacitors, test cells were assembled into two-electrode cells with a TiO_2–(reduced graphene oxide) anode, an AC cathode, a separator (Celgard 2400), and an electrolyte of lithium hexafluorophosphate (1 M) in a 1:1 mixture of ethylene carbonate and dimethyl carbonate (Techno Semichem) in a glove box. As control groups for the TiO_2–(reduced graphene oxide) anode, electrodes were prepared with a mixture of battery-grade commercial TiO_2 powder (Sigma Aldrich, <25 nm) or TiO_2 nanoparticles synthesized without reduced graphene oxide (80 wt%), conductive carbon (10 wt%), and PVDF (10 wt%). Galvanostatic charge–discharge data and CV data at different scan rates were obtained from 1.0 to 3.0 V using a multichannel potentiogalvanostat (WonATech). Electrochemical impedance spectroscopy (EIS) was performed using a ZIVE SP2 electrochemical workstation (WonATech). The cell-discharge capacitance (C_{cell}) was calculated using the relationship $C_{cell} = (i\,t/\Delta V)$, and the specific discharge capacitance (C_{sp}) was calculated from $C_{sp} = (4C_{cell}/m)$,[39,44] where i is the applied current (A), t is the discharge time (s), m is the total mass (g) of active materials in both the anode and cathode, and ΔV is the potential difference (V).

Supporting Information

Supporting Information is available from the Wiley Online Library or from the author.

Acknowledgements

This work was supported by (i) the Energy Efficiency and Resources R&D program (20112020100070) under the Ministry of Knowledge Economy, Republic of Korea, (ii) the Human Resources Development program (20124010203320) of the Korea Institute of Energy Technology Evaluation and Planning (KETEP) grant, which was funded by the Korean government through the Ministry of Trade, Industry and Energy., (iii) the National Research Foundation of Korea Grant Funded by the Korean Government (MEST) (NRF-2009-0094219), and (iv) the Converging Research Center Program through the Ministry of Education, Science and Technology (2012K001267).

Received: May 1, 2013
Revised: May 28, 2013
Published online: June 27, 2013

[1] K. Kang, Y. S. Meng, J. Bréger, C. P. Grey, G. Ceder, *Science* **2006**, *311*, 977.
[2] D. Kalpana, K. Karthikeyan, N. G. Renganathan, Y. S. Lee, *Electrochem. Commun.* **2008**, *10*, 977.
[3] Y.-M. Chiang, *Science* **2010**, *330*, 1485.
[4] H. Kim, H.-D. Lim, S.-W. Kim, J. Hong, D.-H. Seo, D.-c. Kim, S. Jeon, S. Park, K. Kang, *Sci. Rep.* **2013**, *3*, 1506.
[5] P. Poizot, S. Laruelle, S. Grugeon, L. Dupont, J. M. Tarascon, *Nature* **2000**, *407*, 496.
[6] P. Simon, Y. Gogotsi, *Nat. Mater.* **2008**, *7*, 845.
[7] W.-M. Zhang, X.-L. Wu, J.-S. Hu, Y.-G. Guo, L.-J. Wan, *Adv. Funct. Mater.* **2008**, *18*, 3941.
[8] Y. Shi, B. Guo, S. A. Corr, Q. Shi, Y.-S. Hu, K. R. Heier, L. Chen, R. Seshadri, G. D. Stucky, *Nano Lett.* **2009**, *9*, 4215.
[9] K.-F. Hsu, S.-Y. Tsay, B.-J. Hwang, *J. Mater. Chem.* **2004**, *14*, 2690.
[10] L.-Q. Mai, F. Yang, Y.-L. Zhao, X. Xu, L. Xu, Y.-Z. Luo, *Nat. Commun.* **2011**, *2*, 381.
[11] X. Ji, S. Evers, R. Black, L. F. Nazar, *Nat. Commun.* **2011**, *2*, 325.
[12] X. Lu, G. Wang, T. Zhai, M. Yu, J. Gan, Y. Tong, Y. Li, *Nano Lett.* **2012**, *12*, 1690.
[13] G. Zheng, Y. Yang, J. J. Cha, S. S. Hong, Y. Cui, *Nano Lett.* **2011**, *11*, 4462.
[14] Y. Zhai, Y. Dou, D. Zhao, P. F. Fulvio, R. T. Mayes, S. Dai, *Adv. Mater.* **2011**, *23*, 4828.
[15] E. Yoo, H. Zhou, *ACS Nano* **2011**, *5*, 3020.
[16] Y. He, W. Chen, X. Li, Z. Zhang, J. Fu, C. Zhao, E. Xie, *ACS Nano* **2012**, *7*, 174.
[17] L. Lai, H. Yang, L. Wang, B. K. Teh, J. Zhong, H. Chou, L. Chen, W. Chen, Z. Shen, R. S. Ruoff, J. Lin, *ACS Nano* **2012**, *6*, 5941.
[18] K. Naoi, S. Ishimoto, J.-i. Miyamoto, W. Naoi, *Energy Environ. Sci.* **2012**, *5*, 9363.
[19] M.-J. Deng, J.-K. Chang, C.-C. Wang, K.-W. Chen, C.-M. Lin, M.-T. Tang, J.-M. Chen, K.-T. Lu, *Energy Environ. Sci.* **2011**, *4*, 3942.
[20] P. J. Hall, M. Mirzaeian, S. I. Fletcher, F. B. Sillars, A. J. R. Rennie, G. O. Shitta-Bey, G. Wilson, A. Cruden, R. Carter, *Energy Environ. Sci.* **2010**, *3*, 1238.
[21] Q. Wang, Z. H. Wen, J. H. Li, *Adv. Funct. Mater.* **2006**, *16*, 2141.
[22] F. Gao, Z. Tang, *Electrochim. Acta* **2008**, *53*, 5071.
[23] N. Balke, S. Jesse, A. N. Morozovska, E. Eliseev, D. W. Chung, Y. Kim, L. Adamczyk, R. E. Garcia, N. Dudney, S. V. Kalinin, *Nat. Nanotechnol.* **2010**, *5*, 749.
[24] S. Stewart, P. Albertus, V. Srinivasan, I. Plitz, N. Pereira, G. Amatucci, J. Newman, *J. Electrochem. Soc.* **2008**, *155*, A253.
[25] S. W. Lee, N. Yabuuchi, B. M. Gallant, S. Chen, B.-S. Kim, P. T. Hammond, Y. Shao-Horn, *Nat. Nanotechnol.* **2010**, *5*, 531.
[26] J. Han, L. L. Zhang, S. Lee, J. Oh, K.-S. Lee, J. R. Potts, J. Ji, X. Zhao, R. S. Ruoff, S. Park, *ACS Nano* **2013**, *7*, 19.
[27] H.-G. Jung, N. Venugopal, B. Scrosati, Y.-K. Sun, *J. Power Sources* **2013**, *221*, 266.
[28] D. Cericola, P. Novák, A. Wokaun, R. Kötz, *Electrochim. Acta* **2011**, *56*, 8403.
[29] N. Li, G. Liu, C. Zhen, F. Li, L. Zhang, H.-M. Cheng, *Adv. Funct. Mater.* **2011**, *21*, 1717.
[30] J. S. Chen, Y. L. Tan, C. M. Li, Y. L. Cheah, D. Luan, S. Madhavi, F. Y. C. Boey, L. A. Archer, X. W. Lou, *J. Am. Chem. Soc.* **2010**, *132*, 6124.
[31] J. Ye, W. Liu, J. Cai, S. Chen, X. Zhao, H. Zhou, L. Qi, *J. Am. Chem. Soc.* **2010**, *133*, 933.
[32] J.-Y. Shin, D. Samuelis, J. Maier, *Adv. Funct. Mater.* **2011**, *21*, 3464.
[33] A. A. Belak, Y. Wang, A. Van der Ven, *Chem. Mater.* **2012**, *24*, 2894.
[34] H. Kim, D.-H. Seo, S.-W. Kim, J. Kim, K. Kang, *Carbon* **2011**, *49*, 326.
[35] S.-W. Kim, T. H. Han, J. Kim, H. Gwon, H.-S. Moon, S.-W. Kang, S. O. Kim, K. Kang, *ACS Nano* **2009**, *3*, 1085.
[36] B. D. Cullity, C. R. Stock, *Elements of X-ray Diffraction*, 3rd ed., Prentice Hall, Upper Saddle River, NJ **2001**.
[37] H. Kim, S.-W. Kim, J. Hong, Y.-U. Park, K. Kang, *J. Mater. Res.* **2011**, *26*, 2665.
[38] H. Kim, S.-W. Kim, J. Hong, H.-D. Lim, H. S. Kim, J.-K. Yoo, K. Kang, *J. Electrochem. Soc.* **2011**, *158*, A930.
[39] G. Li, L. Li, J. Boerio-Goates, B. F. Woodfield, *J. Am. Chem. Soc.* **2005**, *127*, 8659.
[40] V. Aravindan, Y. L. Cheah, W. F. Mak, G. Wee, B. V. R. Chowdari, S. Madhavi, *ChemPlusChem* **2012**, *77*, 570.
[41] K. Karthikeyan, S. Amaresh, V. Aravindan, H. Kim, K. S. Kang, Y. S. Lee, *J. Mater. Chem. A* **2013**, *1*, 707.
[42] V. Subramanian, A. Karki, K. I. Gnanasekar, F. P. Eddy, B. Rambabu, *J. Power Sources* **2006**, *159*, 186.
[43] X.-H. Xia, J.-P. Tu, X.-L. Wang, C.-D. Gu, X.-B. Zhao, *Chem. Commun.* **2011**, *47*, 5786.
[44] T. Brezesinski, J. Wang, S. H. Tolbert, B. Dunn, *Nat. Mater.* **2010**, *9*, 146.
[45] V. Aravindan, W. Chuiling, M. Reddy, G. S. Rao, B. Chowdari, S. Madhavi, *Phys. Chem. Chem. Phys.* **2012**, *14*, 5808.
[46] J.-Y. Luo, Y.-Y. Xia, *J. Power Sources* **2009**, *186*, 224.
[47] V. Aravindan, W. Chuiling, S. Madhavi, *J. Mater. Chem.* **2012**, *22*, 16026.
[48] N. J. Dudney, *Electrochem. Soc. Interfaces* **2008**, *17*, 44.
[49] W. Li, J. R. Dahn, D. S. Wainwright, *Science* **1994**, *264*, 1115.
[50] A. Chu, P. Braatz, *J. Power Sources* **2002**, *112*, 236.
[51] Y.-G. Guo, Y.-S. Hu, W. Sigle, J. Maier, *Adv. Mater.* **2007**, *19*, 2087.
[52] F.-F. Cao, Y.-G. Guo, S.-F. Zheng, X.-L. Wu, L.-Y. Jiang, R.-R. Bi, L.-J. Wan, J. Maier, *Chem. Mater.* **2010**, *22*, 1908.
[53] C. Jiang, E. Hosono, H. Zhou, *Nano Today* **2006**, *1*, 28.
[54] W. S. Hummers, R. E. Offeman, *J. Am. Chem. Soc.* **1958**, *80*, 1339.